Optical, Structural and Magnetic Properties of Copper-doped Iron Ferrite Synthesized by a Sol-Gel Method *

Dr. Nasser K. Hejazy ∗∗

Prof. Talaat M. Hammad ∗∗∗

Abstract:

The samples of $Cu_xFe_{2-x}O4$ (x = 0.0, 0.2, 0.4, 0.6, 0.8 and 1.0) ferrites were synthesized by a sol-gel method. The structural, morphological, optical and magnetic properties of the products were determined and characterized in detail by X-Ray Diffraction (XRD), Fourier transform infrared spectroscopy (FT-IR), Transmission Scanning Electron Microscopy (TEM), Energy Dispersive X-ray spectroscopy (EDX) and Superconducting Quantum Interferometer Device (SQUID). X-ray analysis showed that all compositions crystallize with a cubic spinel-type structure with an average crystallite size in the range of 11–13 nm. The lattice parameter increased from 8.30 to 8.400 Å with increasing Zn content. The optical properties of the nano-ferrites were investigated by UV–vis spectroscopy and photoluminescence (PL) spectra. UV–vis absorption spectra show that the energy band gap (E_g) of Zn-doped copper ferrite decreases from 3.64 to 3.10 eV when the particle size is increased. The broad visible emission band is observed in the entire PL spectrum. The $Cu_xFe_{2-x}O4$ nano-ferrites exhibit super-paramagnetic behavior at room temperature (RT).

Keywords: Nanostructures; Optical Properties; Magnetic Properties; Ferrites

تحديد الخواص التركيبية والمورفولوجية والبصرية والمغناطيسية لفريت النحاس المحضر بتقنية Sol-Gel

ملخص:

تم تصنيع مركبات حديديك من نوع $Cu_xFe_{2-x}O_4$ (x = 0.0, 0.2, 0.4, 0.6, 0.8 and 1.0) باستخدام طريقة سول–جل. تم تحديد الخواص التركيبية والمورفولوجية والبصرية والمغناطيسية للمنتجات وتميزها بالتفصيل عن طريق حيود الأشعة السينية (XRD) ، والتحليل الطيفي بالأشعة تحت الحمراء من (FT-IR) ، والتحليل الإلكتروني المجهر الضوئي (TEM) ، والأشعة السينية المشتتة للطاقة (Energy Dispersive X-ray) والتحليل الطيفي (EDX) وجهاز قياس التداخل الكمي فائق التوصيل (SQUID) . أظهرت تحاليل الأشعة السينية أن جميع التركيبات تتبلور مع بنية من نوع الإسبنيل مكعب

مع متوسط حجم البللوريت في نطاق 13.11 نانومتر. زاد معامل الشبيكه من 8.331 إلى 8.400 Å مع زيادة محتوى النحاس. تم فحص الخواص الضوئية للعينات عن طريق الأشعة فوق البنفسجية مقابل التحليل الطيفي والأطياف الضوئية (PL). تظهر أطياف الامتصاص تجاه الأشعة فوق البنفسجية أن فجوة نطاق الطاقة (Eg) لفريت النحاس النانومترية تنخفض من 3.64 إلى eV 3.10 عند زيادة حجم الجسيم. لوحظ نطاق البث المرئي العريض في الطيف PL بأكمله. ويظهر المعيار النانوي $Cu_xFe_{1-x}O4$ سلوكًا مغناطيسيًا فائقًا عند درجة حرارة الغرفة (RT).

الكلمات المفتاحية: بنية نانوية، الخواص البصرية، الخواص المغناطيسية، الفريت

Introduction

Copper Ferrite ($CuFe_2O_4$) nanoparticles are considered one of the most interesting metal-oxide materials because of their unique magnetic properties [1]. Consequently, they were successfully used in many applications such as high-density magnetic recording [2], ferrofluids technology [3], biomedical drug delivery [4], magnetic resonance imaging [5], data storage, biosensors [6], biocompatible magnetic nanoparticles for cancer treatment [7], and magneto-optical devices [8]. Spinel ferrites with the general formula MFe_2O_4 (M = Cu, Mn, Mg, Zn, Ni, Co, etc.) have remarkable magnetic, catalytic, optical, and electrical properties [9]. In particular, copper ferrite ($CuFe_2O_4$) is an important material for understanding the behavior of all spinel ferrites. The structure of copper ferrite is a cubic close-packed arrangement of oxygen ions with Cu^{2+} and Fe^{3+} ions in two different sites, vis. tetrahedral (A-site) and octahedral (B-site) oxygen coordination [10]. The structure is neither the spinel nor the inverse spinel structure, but it is a disordered structure containing both types of ions in both types of sites [11].

This work reports the effect of Cu-doping on structural, optical and magnetic properties of $Cu_xFe_{2-x}O_4$ (x = 0.0, 0.2, 0.4, 0.6, 0.8 and 1.0) nano-ferrite prepared by a sol-gel chemical method. Various characterization techniques have been carried out using X-Ray Diffraction (XRD), Transmission Electron Microscopy (TEM), Energy Dispersive X-ray spectroscopy (EDX),

Optical, Structural and Magnetic Properties
of Copper-doped Iron Ferrite Synthesized by a Sol-Gel Method

Dr. Nasser K. Hejazy
Prof. Talaat M. Hammad

UV–vis spectroscopy, photoluminescence (PL) spectra, Superconducting Quantum Interferometer Device (SQUID) techniques and the results are presented herein.

Materials and Methods

All chemicals were of analytical grade and were used without further purification. High purity $Fe(NO_3)_3.9H_2O$, $Cu(NO_3)_2.6H2O$ Alcoholic solution, butanol Renex 95, and liquid paraffin (Nujol®) were purchased from Sigma Aldrich.

Synthesis of pure and Cu-doped Iron Ferrites Nanoparticles

It is well known that additives play an important role in improving the magnetic characteristics of ferrites. In the present research, we study the effect of Cu-doping on structural, optical and magnetic properties of iron ferrites. Iron ferrites and Cu-doped iron ferrites ($0.2 \leq x \leq 1.0$) nanoparticles are prepared by sol-gel method. ($Fe(NO_3)_3.9H_2O$) and copper nitrate ($Cu(NO_3)_2.6H2O$) powders with a Fe: Cu mole ratio of (x):(1-x) (with x = 0.0, 0.2, 0.4, 0.6, 0.8 and 1.0)) were dissolved, in butanol, and were prepared and heated under stirring to 90°C. So, using 8 mL of concentrated surfactant Renex 95®, another solution of concentrated ammonia was prepared containing 4% (in volume) of surfactant (Renex 95®). The ammonia solution was added drop by drop to the iron III solution to promote precipitation of iron oxi-hydroxide. The precipitate was centrifuged and washed with butanol containing 4% (in volume) of surfactant at 90°C in order to eliminate the ammonium chloride as much as possible. After five washing cycles, we observed the precipitation and formation of 100 mL of true solution. Subsequently, 8 mL of surfactant (Renex 95®) and 10 mL of liquid paraffin (Nujol®) were added to the sol. The sol was dried at 70°C under stirring to aid butanol evaporation. Therefore, a viscous dark liquid was obtained. The viscous dark liquid was dried in a hermetically closed sintering chamber at 250°C under N2 pressure (2 atm) for a half-hour until the gel dried into the form of a powder. The prepared powder samples were then annealed for 5 hours at 500 oC in order to enhance the crystallinity.

The UV–vis absorption spectra of ethanolic nanoparticle solutions resulting from sonication of the products in ethanol were obtained using a Hewlett Packard 8453 spectrometer. The fluorescence measurements were also made on ethanolic solutions of nanoparticles, through a Perkin- Elmer LS 50B luminescence spectrometer calibrated at a 320 nm excitation wavelength. The TEM analysis was conducted through a Tecnai F300 transmission electron microscope, and images were taken after suspending the nanoparticles in ethanol. Crystal structure identification and crystal size analysis were performed by an X-Ray diffractometer XDS 2000, Scintac Inc., USA through CuKα radiation source and scan rate of 2o/min. FT-IR spectra of ferrite nanoparticles were recorded on Frontier (Perkin Elmer) spectrophotometer within a frequency range of 4000–500 cm^{-1}. The samples were mixed with anhydrous KBr and pressed into a pallet. Magnetic characterization was carried out using a SQUID quantum design MPMS XL-7 magnetometer in RSO mode. The magnetic hysteresis loop was observed in the range of -60,000 Oe <H< 60,000 Oe at room temperature.

Results and Discussion

Functional groups of the synthesize $Cu_xFe_{2-x}O_4$ are investigated by FTIR spectroscopy in the range of 500 to 4000 cm^{-1}. By means of infrared radiation, the study of atomic/molecular vibrations and their strengths was an excellent fingerprint for identifying the local chemical bonds [12]. To investigate the structural properties of spinel ferrite, we studied FT-IR spectra of pure and Cu-doped iron ferrite nanopowders as shown in Fig. 1. The broad metal–oxygen bands are seen in the FT-IR spectra of all spinels, and ferrites in particular. These bands are generally observed in the range of 600–500 cm^{-1} [13]. The broad peak in the range of 3200-3700 cm^{-1} appears due to stretching vibration of O-H. The bands at 1623cm-1 and at 2357 cm^{-1} are due to the C-O stretching mode arising from the adsorption of atmospheric CO_2 on the surface of the nanoparticles [14]. The peaks near 1370 cm^{-1} and 1645 cm-1 arise due to the bending vibration of N-O and H-O-H bonds, respectively [15]. The transmission band (~ 585 cm^{-1}) corresponds to the stretching vibrations of metal ions.
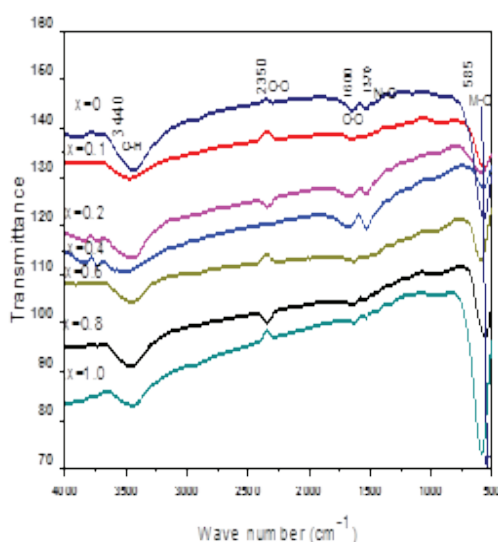
Fig. 1. FTIR spectra of $Cu_xFe_{2-x}O_4$ (x = 0.0, 0.2, 0.4, 0.6, 0.8 and 1.0) nanoferrite

Symmetry is important in the study of structural and optical properties of the nanoparticle ferrites. Samples of pure copper ferrite and zinc-doped copper ferrite $Cu_xFe_{2-x}O_4$ (x = 0.0, 0.2, 0.4, 0.6, 0.8 and 1.0) have been investigated through using X- ray diffraction in the range of 2θ between 25° and 70° and are shown in Fig. 2. The observed peaks at 29.9^o, 35.48^o, 43.76^oo, 53.88^o, 56.79^oo, and 62.34^o can be assigned to the reflections of (220), (311), (400), (422), (511) and (440) crystal planes, respectively. The peaks could be indexed as (220), (311), (400), (422), (511) and (440) which are characteristics of single-phase cubic spinel structure of $CuFe_2O_4$ (ICDD cardno:72-1174) and Fe_2O_4 (ICDD card no: 89-1012). The largest peak of all samples is observable at $2\theta= 35.48^o$. In this work, the XRD results are similar with the XRD results of $CuFe_2O_4$ nanoparticles [16]. All observed XRD peaks could be assigned to a cubic spinel lattice indicating their single phase structure with no other impurity phases (e.g. Fe_2O_3, ZnO, CuO etc.). The intensity of the main diffraction peak of cubic spinel ferrite at the (311) plane was considered as a measure of its degree of crystallinity. The average crystallite size of CuxFe2-xO4 samples was calculated by using the Debye Scherrer formula,

$$D = \frac{k\lambda}{(B\cos\theta)} \qquad (1)$$

The average crystallite size of samples was in the range of 11–13 nm, which are tabulated in table 1.

The lattice constant for each peak of each sample was calculated by using formula (2),

$$a = d\ (h^2 + k^2 + l^2)^{1/2} \qquad (2)$$

where h, k, and l are Miller indices of the crystal planes. It was observed that the lattice constant for each composition increases when increasing Cu substitution and follows Vegard's law (Table 1). This is probably due to the variation of ionic sizes of the Cu^{2+} and Fe^{2+} cations [17-19].
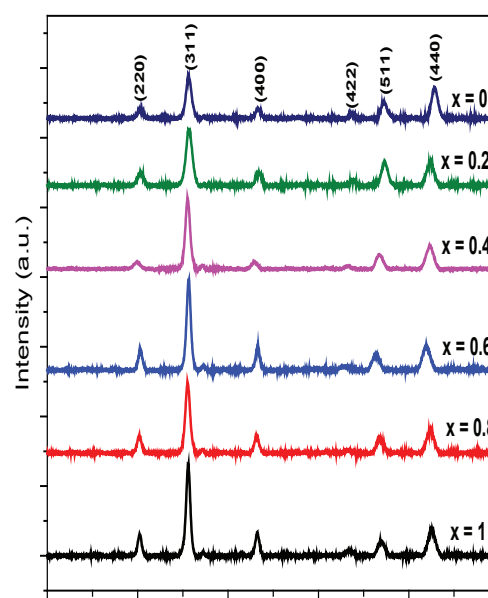

Fig.2. XRD analysis of $Cu_xFe_{2-x}O_4$ nanoferrites.

Table 1.

Average particle size and lattice constants of $Cu_xFe_{2-x}O_4$ nanoparticle

| X	particle size (nm)	lattice constants (Å)
0.0	11.00	8.331
0.2	11.52	8.360
0.4	11.88	8.374
0.6	12.39	8.382
0.8	12 .85	8.388
1.0	13.0	8.4223

TEM is an imaging technique where the system can study small details in the cell or

Optical, Structural and Magnetic Properties
of Copper-doped Iron Ferrite Synthesized by a Sol-Gel Method

Dr. Nasser K. Hejazy
Prof. Talaat M. Hammad

different materials down to near atomic levels [20]. It can investigate the size, shape, and arrangement of the particles which make up the specimen as well as their relationship to each other on the scale of atomic diameters. Fig. 3 (a-d) shows the TEM micrographs and EDX spectrum of $Cu_xFe_{2-x}O_4$ ferrite samples. The figures proved that products are nearly spherical (not uniform) and have the diameter of 15-20 nm, but with agglomeration to some extent, due to the relative higher annealing temperature and interaction between magnetic particles. The agglomeration is due to the Van der Waals force between the particles [21]. The difference in shape and morphologies is correlated with the crystallite dimensions and ionic radii of the precursors. The particle size as seen from the TEM images is slightly different in the XRD technique, because the former is associated with aggregated clusters size, while the latter is associated with the diffracting domains size in the nanoparticles.

Energy Dispersive X-ray spectroscopy (EDX) is an analytical tool used for the elemental analysis and chemical characterization of chemical samples in order to determine their composition. The elemental analysis of $Cu_xFe_{2-x}O_4$ x= (0.0, 0.2, 0.4, 0.6, 0.8 and 1.0) nanostructures was confirmed by (EDX) analysis, and the results are shown in Fig. 3 (a, d). The data show that there is no evidence that other impurities were found and the $CuFe_2O_4$ nanostructures are nearly stoichiometric. These data also confirm the high purity of the $CuFe_2O_4$ nanostructures.
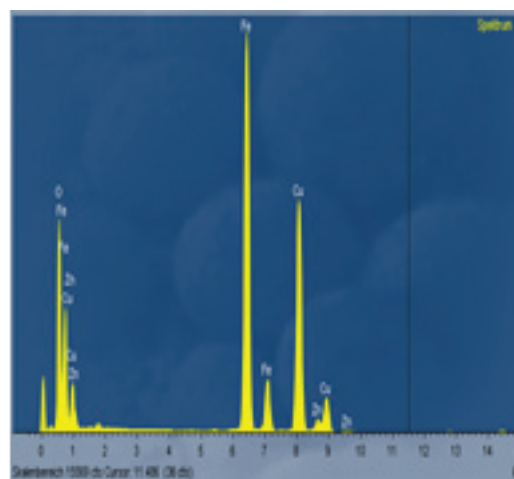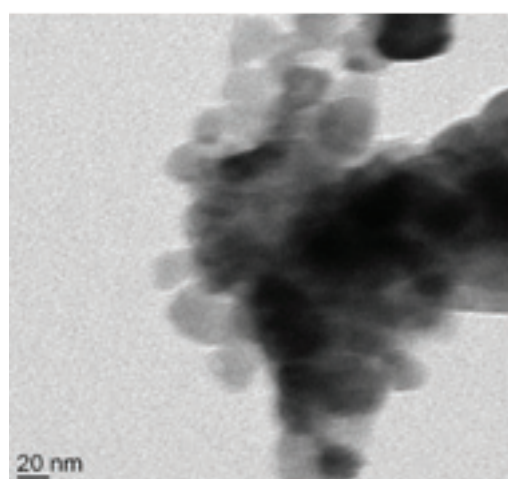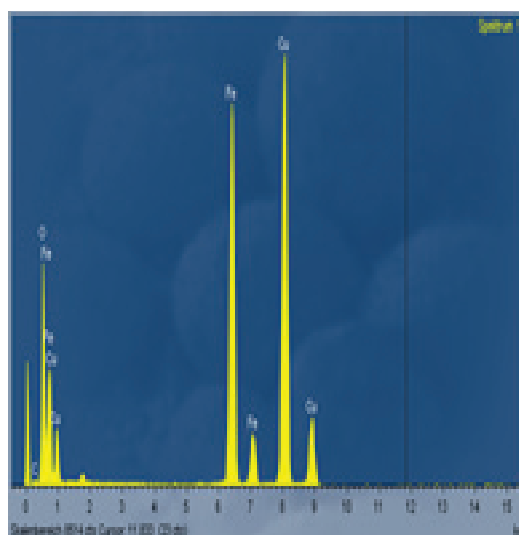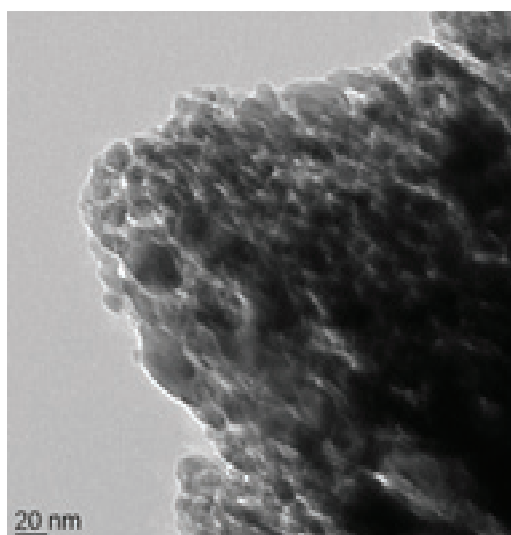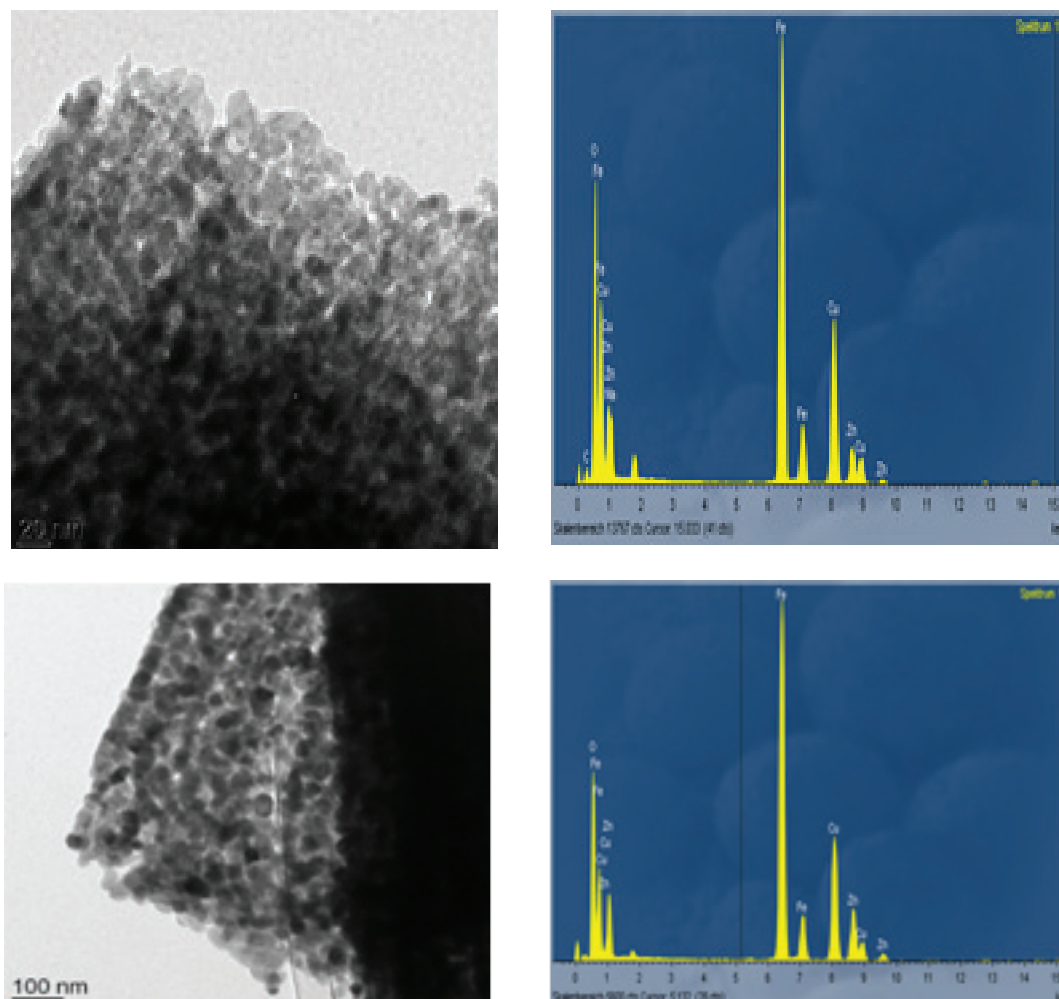
Fig.3. TEM micrographs and EDX spectrum of CxFe2-xO4 (a) x=0.0, (b) x=0.2, (c) x=0.6 and (d) x=1.

UV-vis spectral analysis has been widely used to characterize semiconductor nanoparticles. As the particle size decreases, the absorption edge shifts to shorter wavelength, due to the band gap increase in the smaller particles [21,22]. The absorption spectra of Cu-doped iron ferrite nanoparticles ($Cu_xFe_{2-x}O_4$) in UV-light region is illustrated in Fig. 4. It can be clearly seen that all samples possess an absorption band in the whole range as well as exhibit a good absorption in the light region (330-400 nm). The absorption at 330 nm is assigned to the characteristic absorption band of Fe_2O_4 nanoparticles. On substituting copper in iron ferrites, the absorption band is shifted to longer wavelength as shown in Fig. 4. The fundamental absorption, which corresponds to electron excitation from the valance band to the conduction band, can be used to determine the value of the optical bandgap of the synthesized $Cu_xFe_{2-x}O_4$ ferrite nanoparticles. The optical band gap energies of different compositions are calculated by Tauc's relation, given below [22],

$$(\alpha h v)^{\frac{1}{n}} = A(h v - E_g) \qquad (3)$$

where A is the constant and Eg is the band gap energy of the material and the exponent n depends on the type of transition. For a direct allowed transition n= 1/2, for an indirect allowed transition n= 2, for a direct forbidden n= 3/2 and for an indirect forbidden n= 3. Direct band gap of the samples is calculated by plotting $(\alpha h v)^2$ versus hv and then extrapolating the straight portion of the curve on the hv axis at α = 0. The straight lines plots shown in fig. 5 (a-f) imply that the Cu-doped iron ferrite samples have direct energy band gap and the band gap was present between

Optical, Structural and Magnetic Properties
of Copper-doped Iron Ferrite Synthesized by a Sol-Gel Method

Dr. Nasser K. Hejazy
Prof. Talaat M. Hammad

3.72 to 3.20 eV. The energy gap decreases with the concentration increase of Cu^{+2} due to increase in particle size. On the other hand, the band gap decreases when Cu concentration increases in Fe_2O_4 matrices, although the particle size increases. A similar effect has been observed by Chen et al. [23], Yogo et al. [24] and Wang et al. [25]. The decrease in band gap may also be due to the sp–d exchange interaction between the localized d-electrons of Cu^{2+} ions and band electrons of Fe_2O_4. Thus, the narrowing band gap with Cu-doping could be due to the formation of sub-bands in between the energy band gap and merging of their sub-bands with the conduction band to form a continuous band [26]. This decreases the band gap energy with an increase in Cu content, which may be associated with various parameters such as the crystallite size, structural parameter, carrier concentrations, presence of very small amount of impurities which are not detectable by

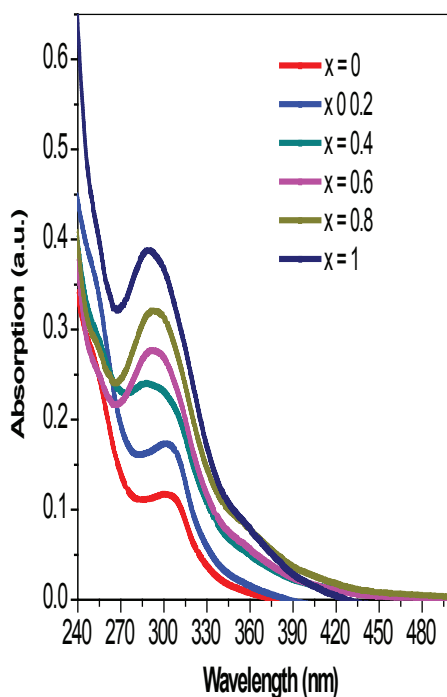XRD and TEM/EDX techniques and lattice strain [27]

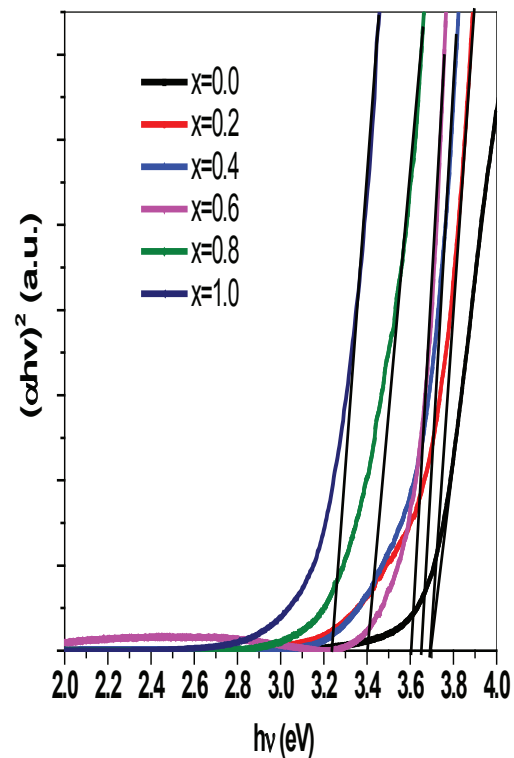**Fig. 5. Energy gap spectra of $Cu_xFe_{2-x}O_4$ nanoferrites**

The photoluminescence (PL) spectra were recorded to investigate the luminescence properties and to obtain the information on band gap with the relative energetic position of sub band gap defect states [28]. Fig. 6 shows the PL spectra at room temperature recorded at the excitation wavelength of 400 nm for all the doped Zn fractions in the copper ferrites. In the present study, un-doped Fe_2O_4 and Cu-doped iron ferrites (x = 0.0, 0. 2, 0. 4, 0. 6, 0. 8, 1.0) show peaks corresponding to blue emissions at 460 nm and green emissions at 510 nm, respectively. The peaks at 460 nm correspond to the blue emissions due to the radiative defects related to the interface traps existing at the grain boundaries [29, 30]. The peak at 510 nm may be attributed to the oxygen vacancies, consequently the green emissions rise [20]. The green emissions peak is commonly referred to as deep-level or trap-state emissions and singly ionized oxygen vacancy [29]. This behavior can be attributed to the

appearance of new electronic levels between the conduction band and the valence band and might be due to the increase of intrinsic defects.
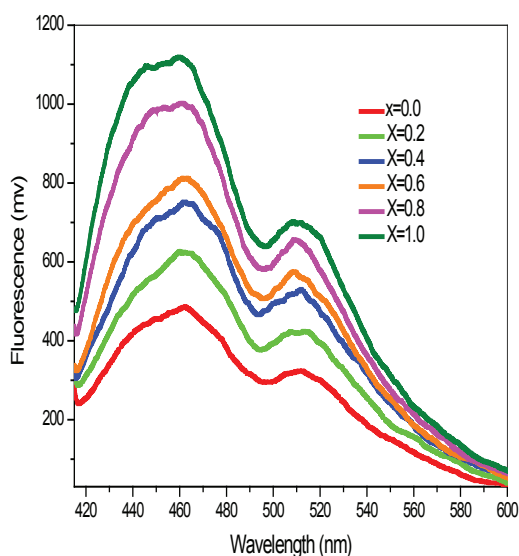

Fig.4. UV-vis. spectra of CuxFe2-xO4 (x= 0.0, 0.2, 0.4, 0.6, 0.8 and 1).

Fig. 6. Photoluminescence spectra of of $Cu_xFe_{2-x}O_4$ (x = 0.0, 0.2, 0.4, 0.6, 0.8 and 1.0) system.

Figure 9 shows the variation of magnetization when field is applied on all four $Cu_xFe_{2-x}O_4$ (x=0, 0.2, 0.4, 0.6, 0.8, 1) nanoferrites. The hysteresis curve (Fig. 7) recorded at room temperature shows very low coercivity and remanence. This proves that particles are superparamagnetic at room temperature.

The saturation magnetization initially increases when copper content increases and reaches a maximum level (70.60 emu/g) for x=0.8. Similar results were reported by Anjaneyulu et al. [30]. This increase is explained by the change in magnetic ion distribution in the spinelic network of copper ferrite where the Fe3+ ions are equally distributed in tetrahedral (A) and octahedral (B) positions. The increase in magnetization up to x=0.8 can be explained using Neel's theory, where Ms = MB-MA. If zinc ion continues to occupy A-sites, the magnitude of A sub-lattice would decrease rapidly which in turn weaken A-B exchange interactions considerably and material may turn paramagnetic. At higher concentrations of copper ions, some of them migrates to the A-site also, which increases the overall saturation of magnetization of the particles. This can also be explained on the basis of Yafet Kittle (spin-canting model), according to which the exchange interaction between A and B sites become lower, which results in strengthening B-B interactions

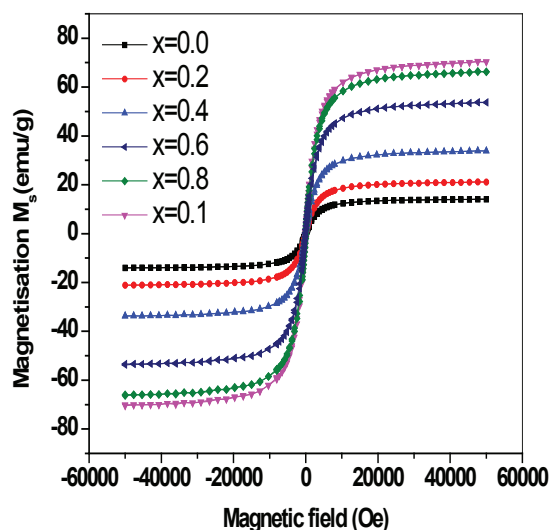and also leads to a decrease in magnetization [31-35]. 3. 72 to 3.20 eV and increase in the particle size.

Fig.7. Magnetic hysteresis loops of $Cu_xFe_{2-x}O_4$ (x = 0.0, 0.2, 0.4, 0.6, 0.8 and 1.0) system.

Conclusions

A series of $Cu_xFe_{2-x}O_4$ (x= 0.0, 0.2, 0.4, 0.6, 0.8 and 1.0) have been successively synthesized by the sol-gel chemical method. The formation of single-phase cubic spinel structure for all compositions was confirmed by XRD. The average crystallite size was calculated by the Debye–Scherrer formula and the range was from 11 to 13 nm. Lattice parameter

was decreased from 8.332 to 8.402Å by increasing Cu^{2+} content. This is due to ionic radius of Cu^{2+} dopant which is smaller than Fe^{2+}. UV–vis spectroscopy shows that the energy band gap (Eg) Cu-doped iron ferrite decreases from 3.72 to 3.20 eV when the particle size is increased.

References

1. X. Meng, H. Li, J. Chen, L. Mei, K. Wang, and X. Li, J. Magn. Magn. Mater. 321 (2009) 1155-1158.

2. M. Sugimoto, The past, present, and future of ferrites, J. Am. Ceram. Soc. 82 (1999) 269-279.

3. M. P. Pileni, Adv. Funct. Mater. 11 (2001) 323-336.

Optical, Structural and Magnetic Properties
of Copper-doped Iron Ferrite Synthesized by a Sol-Gel Method

Dr. Nasser K. Hejazy
Prof. Talaat M. Hammad

4. C. Liu, B. Zou, A. J. Rondinone, and Z. J. Zhang, J. Phys. Chem. B. 104 (2000) 1141-1145.

5. L. Zhen, K. He, C. Y. Xu, and W. Z. Shao, J. Magn. Magn. Mater. 320 (2008) 2672-2675.

6. E. Katz, A.N. Shipway, I. Willner, Nanoparticles, Wiley-VCH Verlag GmbH & Co. KGaA, 2005

7. D.-H. Kim, D. E. Nikles, D. T. Johnson, and C. S. Brazel, J. Magn. Magn. Mater. 320 (2008) 2390-2396.

8. D. Jamon, F. Donatini, A. Siblini, F. Royer, R. Perzynski, V. Cabuil, and S. Neveu, J. Magn. Magn. Mater. 321 (2009) 1148-1154.

9. M. Sugimoto, J. Am. Ceram. Soc. 82, 269–280 (1999)

10. G. F. Goya, H. R. Rechenberg, Nanostruct. Mater. 10, 1001–1011 (1998)

11. E. Prince, E.,R. G. Treuting, Acta Cryst. 9, 1025–1028 (1956).

12. V. A. M. Brabers, J. Phys. Stat. Sol. 33 (1969) 563.

13. R. D. Waldron, Infrared spectra of ferrites, J. Phys. Rev. 99 (1955) 1727.

14. S. B. Qadri, E. F. Skelton, D. Hsu, Dinsmore, A. D. J. Yang, H. F. Gray, J. Physi. Revi.B 60 (1999) 9191.

15. M. J. Iqbal, B. Ismail, J. Allo. Comp. 472 (2009) 434.

16. M. M. Rashad , R. M. Mohamed, M. A. Ibrahim, L. F. M. Ismail, E. A. Abdel-Aal, J. Adva. Powd. Techno. 23 (2012) 315.

17. M. U. Rana, M. U. Islam, T. Abbas, J. Mater. Chem. Phys. 65 (2000) 345.

18. N. Najmoddin, A. Beitollahi, H. Kavas, M.S. Mohseni, H. Rezaie, J. Åkerman, M.S. Toprak, J. Ceram. Int. 40 (2014) 3619.

19. W. Pan, F. Gu, K. Qi, Q. Liu, J. Wang, J. Mater. Chem. Phys. 134 (2012) 1097.

20. K. Maaz, et al., J. Magn. Magn. Mate.308 (2007) 289.

21. G. C. David, K. F. Wayne, E. G. Kenneth, D. M. Gerald, M. Arun, Humphrey, J. Applied Physics, 93 (2003) 793.

22. A. Azam, A. Jawad, A. S. Ahmed, M. Chaman, A. H. Naqvi, J. Alloys Compd. 509 (2011) 2909.

23. Z.C. Chen, L.J. Zhuge, X.M. Wu, Y.D. Meng, Thin Solid Films 515 (2007) 5462.

24. T. Yogo, T. Nakafuku, W. Sakamoto, S.I. Hirano, J. Mater. Res. 20 (2005) 1470.

25. Y.S. Wang, P.J. Thomas, P. O'Brien, J. Phys. Chem. B 110 (2006) 2141211. A. Azam, A. Jawad, A. S. Ahmed, M. Chaman, A. H. Naqvi, J. Alloys Compd. 509 (2011) 2909.

26. A.S. Ahmed, S.M. Muhamed, M.L. Singk, S. Tabassum, A.H. Naqvi, A. Azam, J. Lumin. 131 (2011) 1.

27. R.B. Kale, C.D. Lokhande, Appl. Surf. Sci. 223 (2004) 343.

28. M. U. Rana, M. U. Islam, T. Abbas, J. Mater. Chem. Phys. 65 (2000) 345.

29. N. Najmoddin, A. Beitollahi, H. Kavas, M.S. Mohseni, H. Rezaie, J. Åkerman, M.S. Toprak, J. Ceram. Int. 40 (2014) 3619.

30. W. Pan, F. Gu, K. Qi, Q. Liu, J. Wang, J. Mater. Chem. Phys. 134 (2012) 1097.

31. T. Anjaneyulu, P. Narayana Murthy, Sk. Md. Rafi, Sk. Bademiya, G. Samuel John, Journal of International Letters of Chemistry 14 (2013) 37-43.

32. G.Vaidyanathan, S. Sendhilnathan,   R. Arulmurugan, J. Magn. Magn. Mater. 313 (2007) 293.

33. M. U. Islam, M. U. Rana, T. Abbas, Mater. Chem. Phys. 57 (1998) 190.

34. Y. Yafet, C. Kittle, Phys. Rev. 87 (1952) 290.

35. 35. Y Koseglu, A Baykal, F Gozuak, H Kavas, Polyhedron, 28 (2009) 2887.